Sato *et al. Earth, Planets and Space* (2017) 69:103
DOI 10.1186/s40623-017-0688-1

Earth, Planets and Space

LETTER

Open Access

Morphologies of omega band auroras

Natsuo Sato[1,2*], Akira Sessai Yukimatu[1,2], Yoshimasa Tanaka[1,2] and Tomoaki Hori[3,4]

Abstract

We examined the morphological signatures of 315 omega band aurora events observed using the Time History of Events and Macroscale Interactions during Substorm ground-based all-sky imager network over a period of 8 years. We find that omega bands can be classified into the following three subtypes: (1) classical (O-type) omega bands, (2) torch or tongue (T-type) omega bands, and (3) combinations of classical and torch or tongue (O/T-type) omega bands. The statistical results show that T-type bands occur the most frequently (45%), followed by O/T-type bands (35%) and O-type bands (18%). We also examined the morphologies of the omega bands during their formation, from the growth period to the declining period through the maximum period. Interestingly, the omega bands are not stable, but rather exhibit dynamic changes in shape, intensity, and motion. They grow from small-scale bumps (seeds) at the poleward boundary of preexisting east–west-aligned auroras, rather than via the rotation or shear motion of preexisting east–west-aligned auroras, and do not exhibit any shear motion during the periods of auroral activity growth. Furthermore, the auroral luminosity is observed to increase during the declining period, and the total time from the start of the growth period to the end of the declining period is found to be about 20 min. Such dynamical signatures may be important in determining the mechanism responsible for omega band formation.

Keywords: Omega band aurora, Torch aurora, Tongue aurora, Pulsating aurora, All-sky imager, THEMIS, Ionosphere, Magnetosphere, Field-aligned current

Introduction

Auroral luminosity undulations of the poleward boundaries of diffuse auroras were first described by Akasofu and Kimball (1964) and were named "omega bands" due to the similarity of their shapes to inverted (poleward-opening) versions of the Greek letter Ω. Omega bands are generally observed in the post-midnight and morning sectors during the recovery phases of magnetospheric substorms. They typically have sizes of 400–1000 km and usually drift eastward at speeds of 0.3–2 km/s.

The ionospheric electrodynamic characteristics of omega bands have been described in several papers (see, e.g., Wild et al. 2000, 2011; Syrjäsuo and Donovan 2004; Amm et al. 2005; Vanhamäki et al. 2009, and references therein), all of which support the overall picture of a sequence of upward and downward field-aligned currents (FACs) located in the bright and dark regions, respectively, of such structures. As the band structure with its temporally stationary current system moves above ground-based magnetometers, Ps6-type magnetic pulsations (with periods of 5–40 min) are observed (Saito 1978; Rostoker and Barichello 1980). Omega bands generally consist of intense pulsating auroras (Oguti et al. 1981; Sato et al. 2015). However, the mechanism responsible for omega band formation remains unclear.

The classification of omega bands has gradually evolved. Oguti et al. (1981) and Lyons and Walterscheid (1985) described omega bands as "torch-like" structures extending from the poleward boundaries of post-midnight diffuse auroras. Lühr and Schlegel (1994) described omega bands as "tongue-like" protrusions extending northward.

Unlike auroral arcs, which are indeed the predominant form of auroras, omega bands are observed rather rarely. Consequently, relatively little attention has been paid to omega bands and only a limited number of related reports have been published. Furthermore, satellite images, which can provide larger geographical coverage, had significantly lower spatial and temporal resolution than all-sky TV cameras on the ground. Thus, the main

*Correspondence: nsato@nipr.ac.jp
[1] National Institute of Polar Research, Tokyo, Japan
Full list of author information is available at the end of the article

morphological features of omega bands during formation have not yet been well established. To identify these features, it is important to examine the dynamic and morphological signatures of as many omega band events as possible.

In this study, we analyzed 315 omega band events that were observed using the Time History of Events and Macroscale Interactions during Substorm (THEMIS) ground-based all-sky imager (ASI) network. We examined the optical signatures occurring during the generation of the omega bands, from the growth period to the declining period through the maximum period, and classified the omega bands based on their morphological forms.

Instrumentation

In this study, we employed optical ASI data obtained at the THEMIS ground-based observatories (GBOs) (Angelopoulos 2008; Mende et al. 2008). Combining all of the ground-based THEMIS, ASI data yielded global aurora data, covering broad latitude and longitude ranges with high spatial (~1 km near the zenith) and temporal (3 s) resolutions. The white light all-sky imagers covered a wide wavelength range of about 400–700 nm, and the images were projected onto an ionospheric altitude of 110 km.

To identify "omega band-like" aurora events in this study, we firstly examined a summary plot of the THEMIS data (example of March 1, 2011, <http://themis.ssl.berkeley.edu/gbo/display.py?date=2011.03.01&view_type=summary&submit=Start>) acquired over a period of 8 years, from January 2007 to December 2014. Our selection method is based on a qualitative visual inspection of the images. First, we checked the aurora keogram. Omega band-like events can be easily identified in the keogram because most omega auroras display a "wedge-shaped" or "triangle-shaped" structure with duration of several tens of minutes. Omega band auroras display such peculiar shapes in the keogram and usually drift eastward and cross the meridian plane of ASI (see examples shown in Figs. 2 and 5 of Sato et al. 2015). Subsequently, we analyzed the auroral shapes using a sequence of ASI images to check whether or not the shapes of the auroras looked like omega bands. Finally, we selected 315 events that exhibited the specific characteristics of omega bands. Events whose activity declined before arriving at the meridian plane of ASI were not counted as omega band events.

To examine the morphological and dynamic signatures of the shapes and motions of the omega bands, we produced movie files using the original 3-s-resolution ASI data.

Observations

After selecting the events and obtaining the movie files, we classified the omega bands based on their morphologies and examined the optical characteristics occurring during their generation, from the growth period (the period over which the undulation area increased from the start of the appearance of the protrusions) to the declining period (the period of decreasing or shrinking undulation area and the period over which the undulation loses its omega shape until it disappears all together) through the maximum period (the period over which the spatial size of the omega is at its maximum).

Morphological signatures

Classification of omega bands and their growth signatures

Using the data from the 315 selected events, we determined that omega bands can be classified into the following three subtypes based on the morphological signatures: (1) classical (O-type) omega bands, (2) torch or tongue (T-type) omega bands, and (3) combinations of classical and torch or tongue (O/T-type) omega bands. Figure 1 presents typical examples of the three types of omega bands that we identified. Auroras with O-type bands are diffuse auroras whose poleward boundaries exhibit two undulating shapes resembling inverted versions of the Greek letter Ω (Akasofu and Kimball 1964). Auroras containing T-type omega bands are also diffuse auroras whose poleward boundaries exhibit undulating shapes extending northward; in these cases, the undulating shapes resemble torches or tongues. Although the shapes of torches and tongues are very similar to each other, torches are usually larger and show more rapid movements of their shape and luminosity as compared to tongues, as shown later in Fig. 4 and also in Additional file 3: Movie S3 and Additional file 4: Movie S4. O/T-type omega band auroras exhibit the undulating shapes of both O-type and T-type omega band auroras simultaneously. That is, the boundaries in the dark sections between torches (or tongues) resemble inverted Ω shapes.

Figure 2 presents an example of the growth signature of an O-type omega band aurora, which was observed at Gillam (GILL) in Canada (Mag. Lat. 66.0°, Long. 333.2°) on February 27, 2009. The two undulating shapes of the poleward boundary of the diffuse aurora, which resembles an inverted Ω, become brighter and clearer with time. Notably, the poleward boundary of this aurora contrasts sharply with the dark region, which is located on the poleward side of the undulating aurora. An additional movie file shows this in more detail (see Additional file 1: Movie S1).

Figure 3 provides an example of the growth signature of a T-type aurora. This particular aurora was observed at Gakona (GAKO) in Alaska (Mag. Lat. 63.1°, Long. 269.5°)

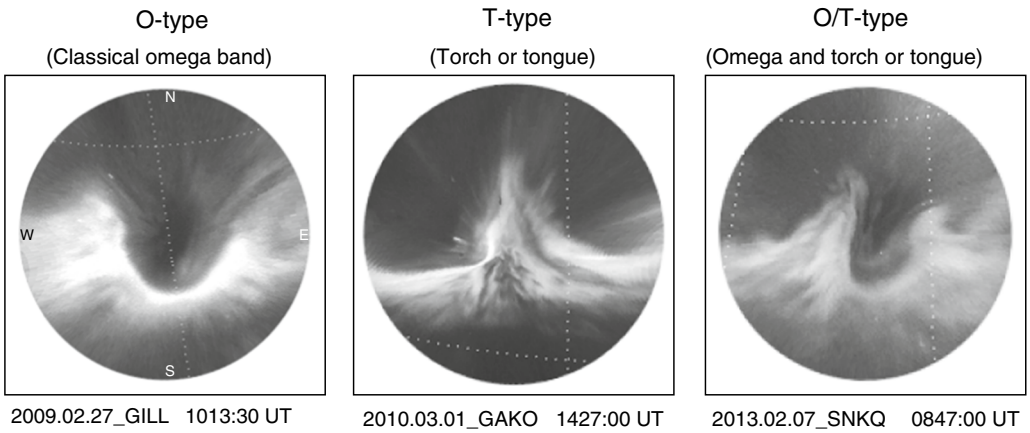

Fig. 1 Examples of (*left*) O-type, (*middle*) T-type, and (*right*) O/T-type omega bands

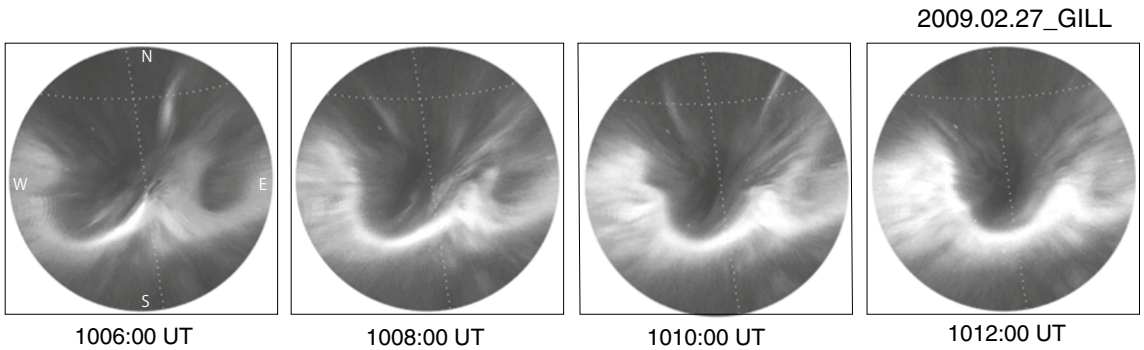

Fig. 2 Typical growth characteristics of an O-type omega band

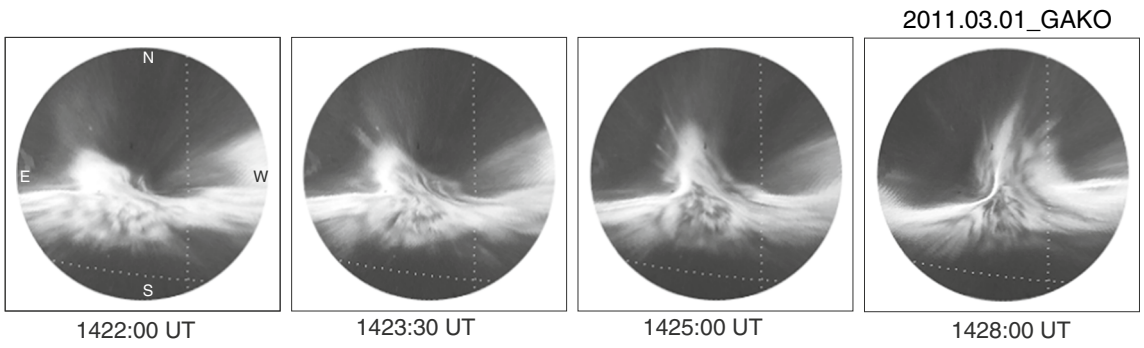

Fig. 3 Typical growth characteristics of a T-type omega band

on March 1, 2011. The poleward boundary of the part of the diffuse aurora in the western portion of the field of view expands poleward with time between 1422:00 UT and 1428:00 UT. Notably, the torch-shaped poleward boundary does not exhibit shear motion, but rather simply extends poleward. It may be important to examine this signature to identify the mechanism responsible for omega band aurora formation. The 3-s-resolution movie corresponding to this event revealed an intense, pulsating aurora consistent with the inside of a torch aurora. An additional movie file shows this in more detail (see Additional file 2: Movie S2).

The upper panels of Fig. 4 depict an O/T-type aurora whose T-type structure is tongue-shaped. This aurora was observed at Kiana (KIAN) in Alaska (Mag. Lat. 65.0°, Long. 251.5°) on October 2, 2011. At 1214:00 UT, the aurora mainly exhibits O-type omega band characteristics, and the size of the dark part of the omega band decreases with time. Meanwhile, the signature of a T-type omega band, which appears in the western portion of the field of view, grows and becomes clearer with time. The characteristics of both O-type and T-type omega bands are observable in the images acquired at 1216:00 UT and 1217:00 UT; in other words, the aurora is an O/T-type omega band aurora at those times. In this case, the tongue-shaped poleward boundary does not rotate, but rather simply extends poleward. An additional movie file shows this in more detail (see Additional file 3: Movie S3). The lower panels of Fig. 4 present another example of an O/T-type omega band aurora. In this event, which was observed at Goose Bay (GBAY) in Canada (Mag. Lat. 60.4°, Long. 23.0°) on March 9, 2008, the T-type structure is torch-shaped. An O-type omega band is evident from 0504:00 UT until 0510:00 UT in the central to western portion of the field of view. Furthermore, a very active torch is observable in the western part of the O-type omega band and drifts eastward. The eastward drift speed between 0504:00 UT and 0510:00 UT is ~800 m/s. An additional movie file shows this in more detail (see Additional file 4: Movie S4).

Figure 5 provides an example of an O&O/T&T-type omega band aurora, which means that O-type, O/T-type, and T-type omega bands all appeared during the same event. The left panel is an image of an O-type omega band aurora that was acquired at GBAY at 0428:00 UT on March 9, 2008. The middle and right panels are images of the O/T-type omega band aurora at 0431:00 UT and the T-type omega band aurora at 0433:00 UT, respectively. The frequencies with which auroras with multiple types of omega bands, namely O&O/T&T-type and O/T&T-type omega band auroras, were observed are provided in Fig. 6. It may be very interesting and important to examine the signatures of such auroras to determine the mechanism responsible for the formation of omega bands. An additional movie file shows this in more detail (see Additional file 5: Movie S5).

Statistics of the observed auroras

Figure 6 illustrates the occurrence rates of the different types of auroras among the 315 selected events. The left panel includes the occurrence rates of all of the possible omega band event types. The total number of events in this chart is 315, and each event can consist of multiple types of omega auroras. For example, O&O/T&T-type means that O-type, O/T-type, and T-type omega bands appeared during one event. As shown, O/T&T-type events occur the most often, with a frequency of 34%

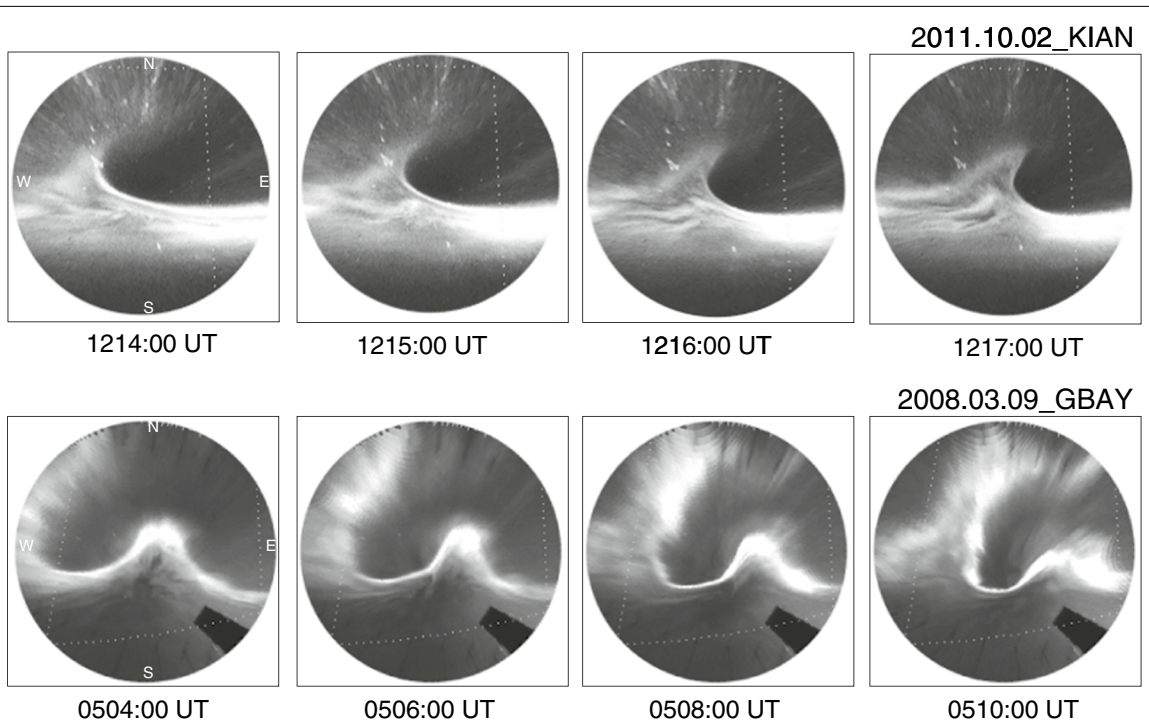

Fig. 4 Typical growth characteristics of O/T-type omega bands in which the T-type structure is that of a tongue (*upper row*) and a torch (*lower row*)

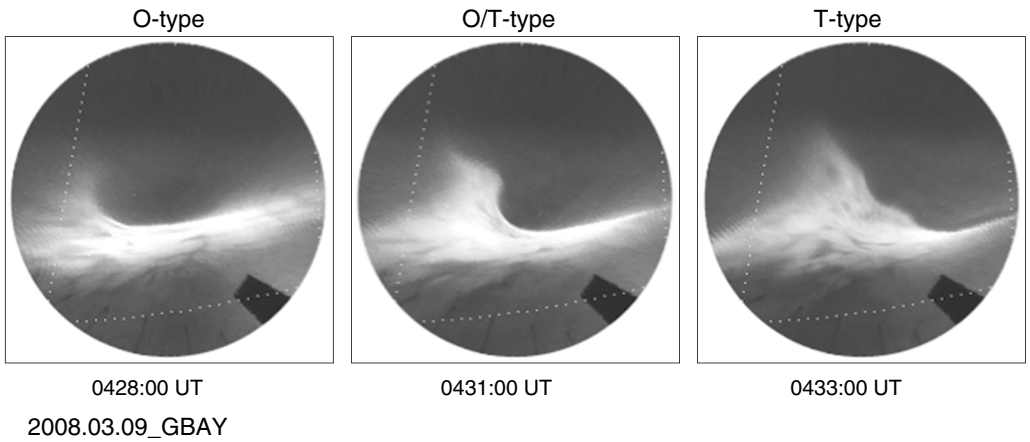

Fig. 5 Example of an O&O/T&T-type omega band event

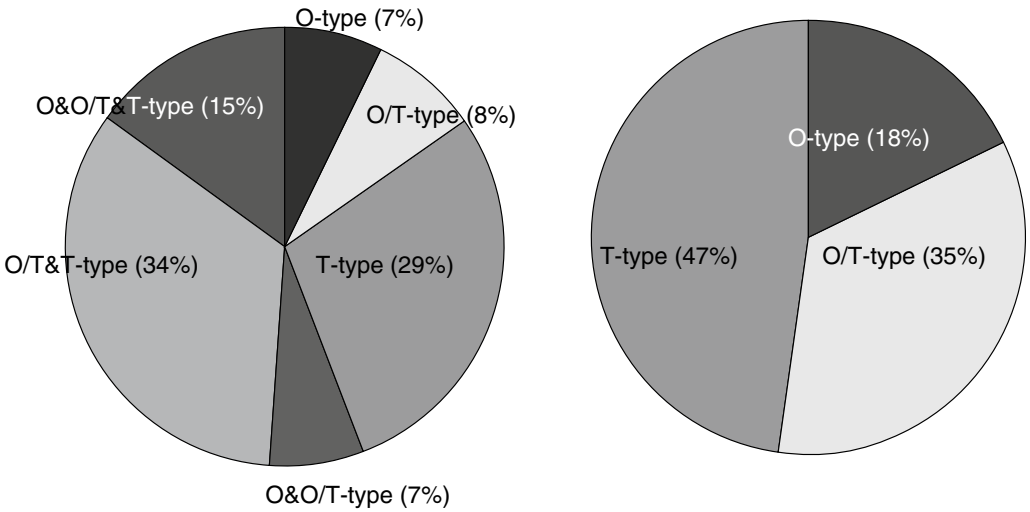

Fig. 6 Occurrence rates of the different aurora types observed in the 315 investigated events, where the *left panel* separately includes events in which multiple omega band types appeared, while the *right panel* shows only the frequencies of the three fundamental omega band types

(104 events), followed by T-type events, which have a frequency of 29% (89 events). O&O/T&T-type, O/T-type, O-type, and O&O/T-type events have frequencies of 15% (46 events), 8% (24 events), 7% (23 events), and 7% (21 events), respectively. On the other hand, the right panel provides the occurrence rates of only the three subtypes of omega bands, O-type, O/T-type, and T-type, as described in the classification. In this statistics, the total number of identified aurora of either type exceeds the total number of events (i.e., periods displaying omega auroras) because multiple types of omega auroras may occur during each event. The results show that O-type, O/T-type, and T-type omega bands occur with frequencies of 18% (90 events), 35% (174 events), and 47% (239 events), respectively. That is, T-type omega bands occur the most often, followed by O/T-type bands and finally O-type bands. It is important to note that when the auroras change their type, they always evolve along the following sequences: from O to O/T, then T-type or from O/T- to T-type. These morphological signatures may be important for the determination of the mechanism responsible for omega band formation.

Life cycles of omega bands from the growth period to the declining period through the maximum period

It is interesting to examine the dynamic signatures of omega band auroras from the growth period to the declining period through the maximum period, examples

of which are presented in Fig. 7. The upper panels depict the event observed at GBAY on March 9, 2008, which is designated as Event 1. Between 0428:00 UT (0051:00 MLT) and 0431:00 UT, the aurora exhibits an O/T-type omega band form, and the torch structure expands with time and drifts eastward. The torch reaches its maximum degree of formation at 0434:00 UT and then dissipates with time between 0442:00 UT and 0443:30 UT. During this declining period, the undulating part at the poleward edge suddenly intensifies in luminosity with more dynamic movement and then gradually disappears. Notably, the auroral luminosity increases during the declining period. Dynamical signatures of this event are shown in Additional file 5: Movie S5. Such signatures could be important to understand the formation mechanism of omega band auroras, as discussed later. The entire process from the start of the growth period to the end of the declining period lasts about 20 min, judging from the original image data (not shown here). The middle panels illustrate the life cycle of the T-type omega band observed during the event at GAKO on March 1, 2011, which is defined as Event 2. The seed of a torch aurora structure appears in the western portion of the east–west-aligned aurora at 1309:00 UT (0224:00 MLT) and expands poleward with time. The torch structure reaches its maximum degree of formation around 1317:00–1321:00 UT and then dissipates with time between 1328:00 UT and 1330:00 UT. During this declining period, the auroral luminosity increases, while the shape is destroyed by 1330:00 UT, as in Event 1. Dynamical signatures of this event are shown in Additional file 6: Movie S6. Again, the duration of the event from the start of the growth period to the end of the declining period is about 20 min, judging from the original image data. The bottom panels show an event similar to Event 2 that was observed at GAKO on March 1, 2011, and is designated as Event 3. The seed of a torch aurora structure appears in the western part of the east–west-aligned aurora at 1420:00 UT (0335:00 MLT). The seed grows with time and expands poleward, forming a torch structure. The torch structure reaches its maximum height of formation between 1420:00 UT and 1427:00 UT and then dissipates with time between 1429:00 UT and 1433:00 UT. As in Events 1 and 2, the aurora luminosity increases with time and the shape is destroyed during the declining period. Dynamical signatures of this event are shown in Additional file 7: Movie

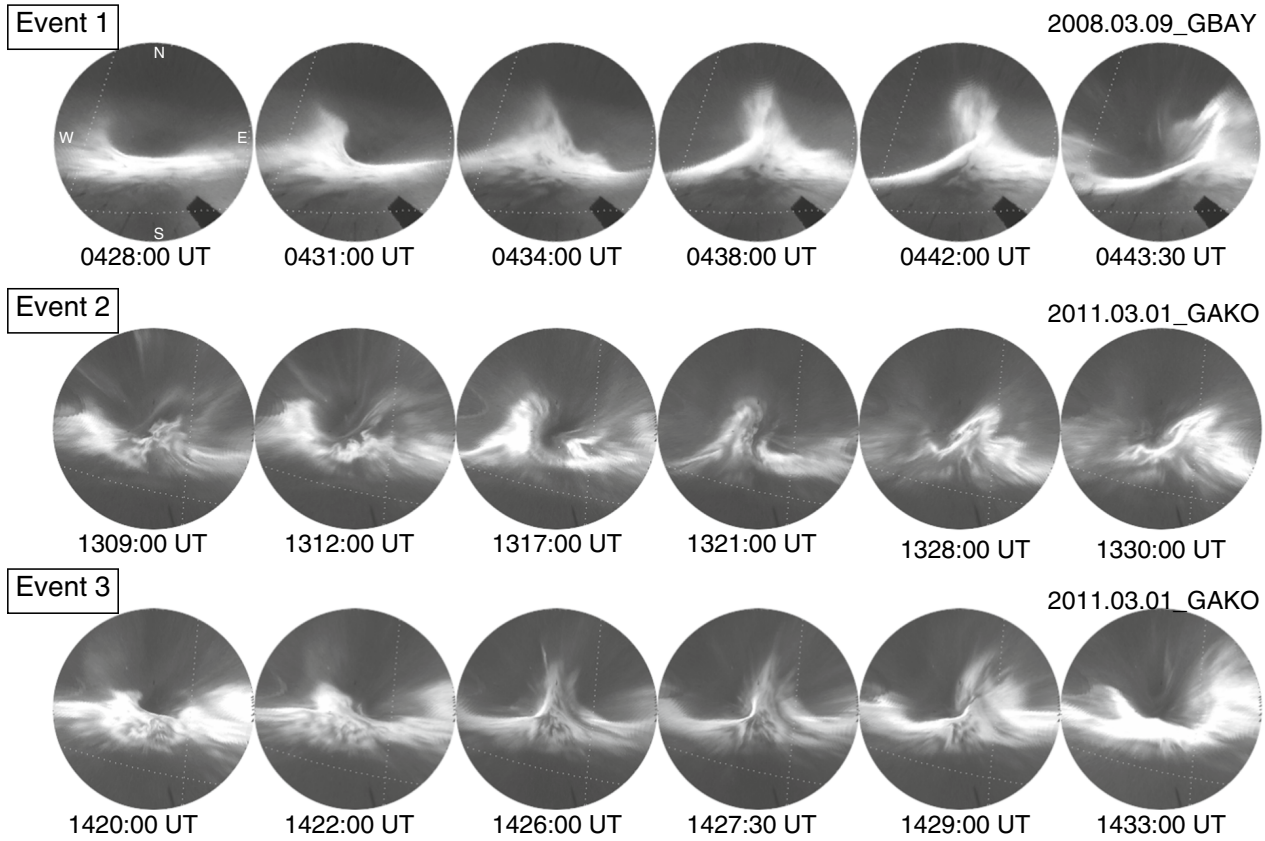

Fig. 7 Images of three events from the growth period to the declining period through the maximum period

S7. The entire event lasts about 20 min from the start of the growth period to the end of the declining period, judging from the original image data.

The statistical results show that about 55% of events occur within a duration of 15–25 min, while 28, 11, and 6% have durations of 25–35, 5–15, and more than 35 min, respectively (not shown). In these statistics, we selected only those events that displayed their entire lifetime from their growth period to their declining period in the field of view of the "single" all-sky imager. We excluded those events where omega auroras drifted outside of the field of view of ASI before full declination of the omega shape. We also excluded those events where omega-shaped auroras appeared from the horizon. Although the background drift speed varies from event to event, typically it takes ~30–40 min for an auroral structure to pass by the field of view of the all-sky camera. Thus, the lifetime of omega band auroras identified here could be bounded by the ~30–40 min of time required for the omega to cross the field of view of the all-sky imager.

Figure 8 presents schematic illustrations of the dynamic signatures from the growth and expansion period to declining period through maximum period. In the left panel, which shows the pattern during the growth and expansion period, the poleward boundary of the east–west-aligned aurora expands with time and forms a tongue or torch shape. The time interval between the dotted line labeled 1 and the solid line designated as line 2 is about 3–5 min. The middle panel, which depicts the pattern during the maximum period of torch or tongue shape formation, shows the poleward boundary extended to its maximum height. In many cases, the maximum period lasts for 2–4 min. In the right panel, which corresponds to the declining period, the poleward boundary of the torch or tongue shape decreases in height and bends eastward with time. The time interval between the dotted line defined as line 4 and the solid line labeled 5 is about 2–5 min. Notably, the auroral intensity often increases during the declining period, as demonstrated in Fig. 7.

Dynamic signatures during the initial phase of the growth of omega bands

Initial growth signatures of omega band auroras provide important information that may be useful in understanding their formation mechanism. However, analysis of these signatures has some limitations due to the fact that such signatures are very complex in most cases, and it is rare to be able to observe a clear, complete shape of omega band auroras near the zenith in field of view of ASI during the initial growth. Under these observational limitations, we have found some examples that demonstrate clear morphological evolutions during the initial growth phase of omega bands, as presented in Fig. 9. The top panels demonstrate the event observed at Kiana (KIAN) in Alaska (Mag. Lat. 65.0°, Long. 251.5°) on March 23, 2007, which is designated as Event 1. The leftmost image at 1405:12 UT (0205:12 MLT) shows east–west-aligned discrete arc auroras, just before the start of omega band auroras. At 1406:54 UT, a small bump/protrusion appears at the poleward boundary of the western part of the preexisting east–west-aligned auroras in the field of view of ASI. Then, this bump expands poleward with time (see panel at 1408:33 UT), and the auroras acquire a tongue-type form at 1410:09 UT. In the images, artificial light contaminates the aurora in the northern part of the image and the artificial light has been masked with a gray area. It is important to note here that the omega band auroras are found to grow from a small-scale bump (a seed) at the poleward boundary of pre-east–west-aligned arc auroras, not via the rotation or shear motion of preexisting east–west-aligned auroras. The second row of images labeled Event 2 shows the growth phase of tongue-type omegas along with intense pulsating auroral patches observed at McGrath (MCCR) in Alaska (Mag. Lat. 61.7°, Long. 260.3°) on March 1, 2011. The leftmost image at 1418:30 UT (0248:30 MLT) demonstrates preexisting east–west-aligned band auroras consisting of pulsating auroras,

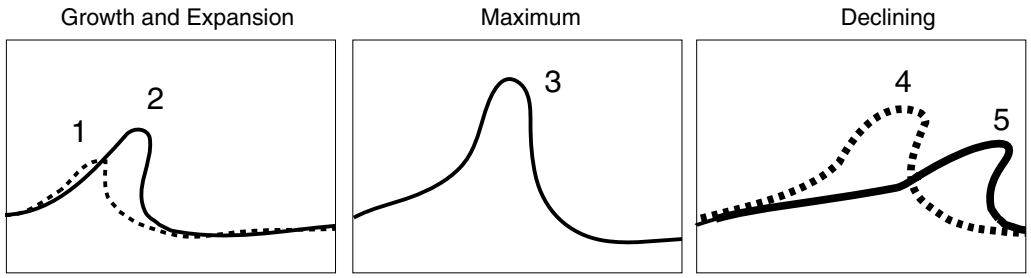

Fig. 8 Schematic depictions of the dynamic signatures of omega band auroras from the growth and expansion period to the declining period through the maximum period

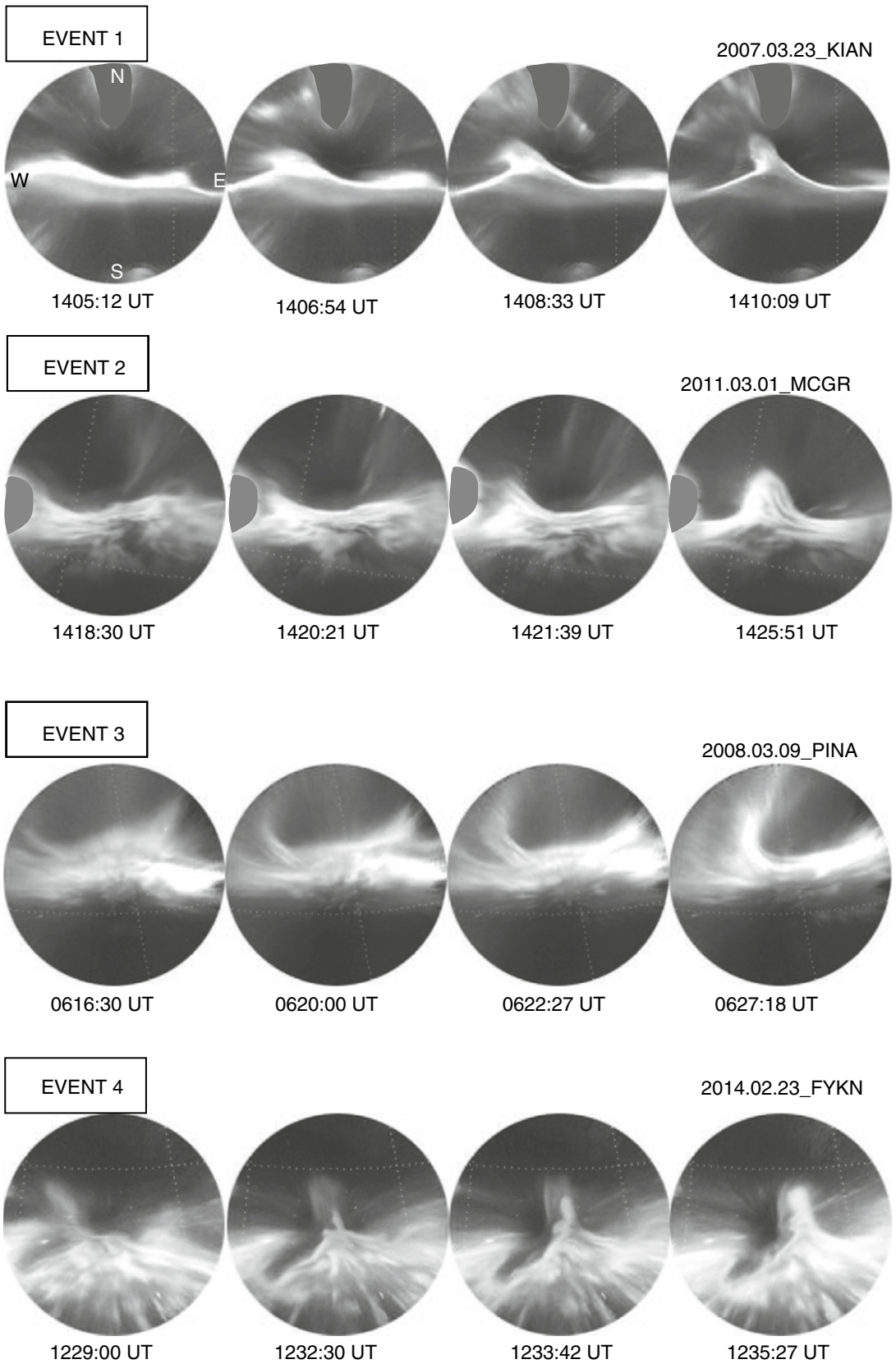

Fig. 9 Images of four events during the initial phase of the growth of omega bands

just before the appearance of the omega band aurora. At 1420:21 UT, a small bump/protrusion appears at the poleward boundary of the western part of the preexisting east–west-aligned band auroras. Then, this bump expands poleward with time and forms the tongue-type omega bands, with a similar behavior as that for Event 1. In these images, artificial light contaminates the western edge. This area has been masked with a gray patch. Dynamical signatures of this event are shown in Additional file 8: Movie S8. The third row panels show the growth signature of torch-type omega bands that were observed at Pinawa (PINA) in Canada (Mag. Lat. 60.0°, Long. 331.9°) on March 9, 2008, and is designated as Event 3. At 0616:30 UT (2339:30 MLT), just before the appearance of the omega band aurora, there are two types of east–west-aligned auroras. One type is the east–west-aligned discrete arc auroras, which are observed on the poleward side. The other type of auroras is observed on the equatorward side forming the east–west-aligned pulsating auroras. At 0620:00 UT, a small-scale torch-like auroral structure (a seed) appears at the western side of the poleward east–west-aligned discrete aurora. Then, the torch-like auroral structure expands poleward and increases in height and intensity with time, as seen at 0622:27 UT and 0627:18 UT. When this torch-type omega aurora reaches a maximum area at about 0627:18 UT, the pulsating auroral regions can be seen embedded within the torch-type omega (see Additional file 9: Movie S9). The bottom panels show the growth signature of omega band auroras consisting of intense patch pulsating auroras that were observed at Fort Yukon (FYKN) in Alaska (Mag. Lat. 67.3°, Long. 266.7°) on February 23, 2014, and is referred to as Event 4. The leftmost panel shows an image at 1229:00 UT (0132:00 MLT), just before the start of the omega band aurora. In this time interval, the intense pulsating auroras cover half of the equatorward region. A weak, non-pulsating auroral element appeared on the western side at the poleward edge of the east–west-aligned pulsating aurora. This weak auroral element drifts eastward as seen in the subsequent images. At 1232:30 UT, the seed of an omega band aurora, which consists of pulsating patches, appears at the poleward side of the east–west-aligned pulsating aurora near the zenith of ASI. This seed grows with time expanding poleward, increasing its intensity, as seen in the images at 1233:42 UT and 1235:27 UT. The growth signatures and the movements of pulsating aurora elements of this event are very similar to the omega event shown in Figs. 3 and 7 of Sato et al. (2015). The dynamics of this event are shown in Additional file 10: Movie S10. It is worth noting here that there are no auroral streamers in any of the events in Fig. 9, and we will discuss this observation later.

Summary and discussion

To the best of the authors' knowledge on the past studies, the main morphological features of omega bands during formation have not yet been well established. In order to identify these features, it is important to examine the dynamic and morphological signatures of as many omega band events as possible. In this study, we have examined morphological signatures of 315 omega band aurora events observed using the THEMIS ground-based ASI network during an 8-year period from January 2007 to December 2014. We have for the first time found that omega bands can be classified as O-type, T-type, and O/T-type bands. Auroras with T-type omega bands occurred the most frequently (45%), followed by those exhibiting O/T-type bands (35%) and finally O-type bands (18%). Accounting for the events in which multiple omega band types appeared, O/T&T-type events were the most common, occurring with a frequency of 34% (104 events), followed by T-type events 29% (89 events). O&O/T&T-type, O/T-type, O-type, and O&O/T-type events occurred with frequencies of 15% (46 events), 8% (24 events), 7% (23 events), and 7% (21 events), respectively.

The reason why the occurrence rate of T-type bands is higher than the rates for other types is not clear at this moment. We need to investigate the relationship between the occurrence of each type of omega band and further examine the occurrence conditions of each type of omega aurora in terms of the magnetic local time, geomagnetic activity, interplanetary magnetic field components (By and Bz), solar wind velocity, ionospheric convection velocity, etc.

Even though identifying the formation mechanisms of omega auroras is beyond the scope of this article, we briefly review previous studies and then make suggestions regarding the mechanisms that may explain the evidence shown in the present work. A number of generation mechanisms, which are reviewed in Amm et al. (2005), have been proposed. The most widely accepted generation mechanisms are that omega bands correspond to waves resulting from a Kelvin–Helmholtz (KH) instability arising in sheared flows in the equatorial regions of the tail (Rostoker and Samson 1984) or the hybrid Kelvin–Helmholtz/Rayleigh–Taylor instability in the plasma sheet (Yamamoto 2011) and, alternatively, that omega bands form as a direct consequence of auroral streamer activity (high-speed flows) in the magnetotail (Henderson 2009, 2012). Weygand et al. (2015) examined these two source mechanisms using the data observed with the THEMIS ground-based observatory and onboard spacecraft. They concluded that the KH instability mechanism could not explain their observational evidence and that the high-speed flow shear mechanism is the most likely

cause of the omega band aurora, but the study lacked observations in regions where the KH instability might have occurred. On the other hand, the auroral streamer mechanism could explain only a fraction of their observational signatures.

In our study with high spatial (~1 km near the zenith) and temporal (3 s) resolution data, we examined the morphological signatures of omega band formation from the growth period to the declining period through the maximum period. Interestingly, the omega bands were observed not to be stable, but rather to exhibit highly dynamical changes in shape, intensity, and motion. We found the following dynamical signatures that may be important to enable determination of the mechanisms responsible for omega band formation: (1) the omega band auroras grow from small-scale bumps (seeds) at the poleward boundary of preexisting east–west-aligned auroras, rather than via the rotation or shear motion of the preexisting east–west-aligned auroras; (2) the auroras did not exhibit any shear motion during the growth of omega auroral activity; (3) the auroral luminosity consistently increased during the declining period; (4) the entire process from the beginning of the growth period to the end of the declining period typically lasted about 20 min; (5) when the auroras changed their type, they always evolved along the following sequences, from O-type to O/T-type, then to T-type or O/T-type to T-type.

It is worth noting that we could not find any auroral streamer events in this study, as shown in Figs. 7 and 9. Because we used single all-sky imager data, there is a possibility that we missed auroral streamer events that prolonged along the north–south direction in the higher latitude region of omega auroras.

During growth and expansion periods of the O-type and O/T-type omega bands, a clear contrast was evident between the regions of light and darkness along the poleward boundaries, which may be the boundaries between the upward and downward FACs, as suggested in previous papers (Lühr and Schlegel 1994; Wild et al. 2000; Amm et al. 2005).

The morphological and dynamical signatures analyzed in this study, especially such characteristics as the highly dynamical changes in shape, intensity, and motion, suggest that the sources of generation and formation of omega bands are not only located near the tail region in the magnetosphere but also the ionosphere may play an important role. That is, the enhancement of auroral luminosity could be caused by the field-aligned acceleration of auroral electrons, which is widely accepted to be caused by magnetosphere–ionosphere coupling processes (Evans 1974; Mozer et al. 1980). A fully magnetospheric model for the formation of omega band auroras may have difficultly explaining the enhancement of auroral luminosity during the declining period, even if it can explain the shape and motion of omega band auroras. Both the KH instability model and auroral streamer model are generation mechanisms that take place in the magnetotail. We strongly propose that the magnetosphere–ionosphere coupling should also play an important role for formation of omega band auroras, especially during the declining period. In order to confirm these generation mechanisms, coordinated observations on the ground and onboard spacecraft located at the equatorial region in the magnetotail and in the ionosphere along the same geomagnetic field lines could be very important.

The statistical signatures of omega band auroras in terms of magnetic local time, duration, recurrence period, drift speed, and relationships to the interplanetary magnetic field components (By and Bz) will be reported in a subsequent article.

Additional files

Additional file 1: Movie S1. Movie data shown in Fig. 2.

Additional file 2: Movie S2. Movie data shown in Fig. 3.

Additional file 3: Movie S3. Movie data shown in the upper panel of Fig. 4.

Additional file 4: Movie S4. Movie data shown in the lower panel of Fig. 4.

Additional file 5: Movie S5. Movie data shown in Fig. 5 and Event 1 shown in Fig. 7.

Additional file 6: Movie S6. Movie data shown in Event 2 of Fig. 7.

Additional file 7: Movie S7. Movie data shown in Event 3 of Fig. 7.

Additional file 8: Movie S8. Movie data shown in Event 2 of Fig. 9.

Additional file 9: Movie S9. Movie data shown in Event 3 of Fig. 9.

Additional file 10: Movie S10. Movie data shown in Event 4 of Fig. 9.

Abbreviations

FAC: field-aligned current; THEMIS: Time History of Events and Macroscale Interactions during Substorm; ASI: all-sky imager; GBO: ground-based observatory; GILL: Gillam; GAKO: Gakona; KIAN: Kiana; GBAY: Goose Bay; IUGONET: Inter-university Upper atmosphere Global Observation NETwork.

Authors' contributions

NS analyzed THEMIS GBO all-sky imager data. TH and YT arranged data analysis software. AY discussed about the ionospheric convection. All authors read and approved the final manuscript.

Author details

[1] National Institute of Polar Research, Tokyo, Japan. [2] SOKENDAI (The Graduate University for Advanced Studies), Kanagawa, Japan. [3] Institute for Space-Earth Environmental Research, Nagoya University, Nagoya, Japan. [4] Department of Earth and Planetary Science, Graduate School of Science, The University of Tokyo, Tokyo, Japan.

Acknowledgements

This work was partially supported by a Grant-in-Aid for Scientific Research C (15K05305), B (25287129) and the Inter-university Upper atmosphere Global Observation NETwork (IUGONET) project funded by the Ministry of Education, Culture, Sports, Science and Technology of Japan. We would like to thank A. Kadokura for useful comments. Part of the work of TH has been conducted at ERG-Science Center (ERG-SC) operated by ISAS/JAXA and ISEE/Nagoya

University. The authors acknowledge NASA contract NAS5-02099 for the use of data from the THEMIS Mission. Specifically, we thank S. Mende and E. Donovan for use of the ASI data. Deployment and data retrieval of the THEMIS ASIs were partly supported by CSA contract 9F007-046101. THEMIS all-sky image data are available through the open data repository at UC Berkeley at http://themis.ssl.berkeley.edu/index.shtml.

Competing interests
The authors declare that they have no competing interests.

Publisher's Note

Received: 27 December 2016 Accepted: 25 July 2017
Published online: 03 August 2017

References

Akasofu SI, Kimball DS (1964) The dynamics of the aurora: I. Instabilities of the aurora. J Atmos Terr Phys 26:205–211
Amm O, Aksnes A, Stadsnes J, Østgaard N, Vondrak RR, Germany GA, Lu G, Viljanen A (2005) Mesoscale ionospheric electrodynamics of omega bands determined from ground-based electromagnetic and satellite optical observations. Ann Geophys 23:325–342
Angelopoulos V (2008) The THEMIS mission. Space Sci Rev 141:5–34. doi:10.1007/s11214-008-9336-1
Evans DS (1974) Precipitating electron fluxes formed by a magnetic field-aligned potential difference. J Geophys Res 79:2853–2858
Henderson MG (2009) Observational evidence for an inside-out substorm onset scenario. Ann Geophys 27:2129–2140
Henderson MG (2012) Auroral substorms, poleward boundary activations, auroral streamers, omega bands, and onset precursor activity, Auroral Phenomenology and Magnetospheric Processes: Earth and Other Planets Geophysical Monograph Series 197, AGU, Washington, D.C., 91–98, 2012. doi:10.1029/2011GM001165
Lühr H, Schlegel K (1994) Combined measurements of EISCAT and the EISCAT magnetometer cross to study omega bands. J Geophys Res 99(A5):8951–8959
Lyons LR, Walterscheid RL (1985) Generation of auroral omega bands by shear instability of the neutral winds. J Geophys Res 90(12):321. doi:10.1029/JA090iA12p12321
Mende SB, Harris S, Frey H, Angelopoulos V, Russell C, Donovan E, Jackel B, Greffen M, Peticolas L (2008) The THEMIS array of ground-based observatories for the study of auroral substorms. Space Sci Rev 141:357–387
Mozer FS, Cattell CA, Hudson MK, Lysak RL, Ternerin M, Torbert RB (1980) Satellite measurements and theories of low altitude auroral particle acceleration. Space Sci Rev 27:155–213
Oguti T, Kokubun S, Hayashi K, Tsuruda K, Machida S, Kitamura T, Saka O, Watanabe T (1981) An auroral torch structure as an activity center of pulsating aurora. Can J Phys 59:1056–1062
Rostoker G, Barichello JC (1980) Seasonal and diurnal variation of Ps 6 magnetic disturbances. J Geophys Res 85:161–163
Rostoker G, Samson JC (1984) Can substorm expansive phase effects arid low frequency Pc magnetic pulsations be attributed to the same source mechanism? Geophys Res Lett 11:271
Saito T (1978) Long-period irregular micropulsations, Pi 3. Space Sci Rev 21:427–467
Sato N, Kadokura A, Tanaka Y, Nishiyama T, Hori T, Yukimatu AS (2015) Omega band pulsating auroras observed onboard THEMIS spacecraft and on the ground. J. Geophys Res Space Phys 120:5524–5544. doi:10.1002/2015JA021382
Syrjäsuo M, Donovan E (2004) Diurnal auroral occurrence statistics obtained via machine vision. Ann Geophys 22:1103–1113
Vanhamäki H, Kauristie K, Amm O, Senior A, Lummerzheim D, Milan S (2009) Electrodynamics of an omega-band as deduced from optical and magnetometer data. Ann Geophys 27:3367–3385
Weygand JM, Kivelson MG, Frey HU, Rodriguez JV, Angelopoulos V, Red-mon R, Barker-Ream J, Grocott A, Amm O (2015) An interpretation of spacecraft and ground based observations of multiple omega band events. J Atmos Solar-Terr Phys 133:185–204. doi:10.1016/j.jastp2015.08.014
Wild JA, Yeoman TK, Eglitis P, Opgenoorth HJ (2000) Multiinstrument observations of the electric and magnetic field structure of omega bands. Ann Geophys 18:99–110
Wild JA et al (2011) Midnight sector observations of auroral omega bands. J Geophys Res 116:A00I30. doi:10.1029/2010JA015874
Yamamoto T (2011) A numerical simulation for the omega band formation. J Geophys Res 116:A02207. doi:10.1029/2010JA015935